Electrochemistry Communications 132 (2021) 107137

Contents lists available at ScienceDirect

Electrochemistry Communications

journal homepage: www.elsevier.com/locate/elecom

A sodium bis(perfluoropinacol) borate-based electrolyte for stable, high-performance room temperature sodium-sulfur batteries based on sulfurized poly(acrylonitrile)

Saravanakumar Murugan [a], Sina V. Klostermann [b], Wolfgang Frey [c], Johannes Kästner [b], Michael R. Buchmeiser [a,d,*]

[a] Institute of Polymer Chemistry, University of Stuttgart, 70569 Stuttgart, Germany
[b] Institute for Theoretical Chemistry, University of Stuttgart, 70569 Stuttgart, Germany
[c] Institute of Organic Chemistry, University of Stuttgart, 70569 Stuttgart, Germany
[d] German Institutes of Textile and Fiber Research (DITF), 73770 Denkendorf, Germany

ARTICLE INFO

Keywords:
Sodium-sulfur batteries
Sulfur-polyacrylonitrile cathode
Bidentate ligands
Weakly coordinating anion
Hydrolysis
Potential energy barrier

ABSTRACT

Sodium bis(perfluoropinacol)borate, $NaB[O_2C_2(CF_3)_4]_2$ (Na-PPB), as part of the electrolyte is introduced to room temperature (RT) sodium-sulfur batteries based on a sulfurized poly(acrylonitrile) (Na-SPAN) cathode. Na-PPB was stable under atmospheric conditions for 20 days and showed no sign of degradation. Na-SPAN full cells based on a Na-PPB electrolyte demonstrated excellent oxidation stability against various current collectors and delivers a high discharge capacity of >950 mAh/g_{sulfur} with 100 % coulombic efficiency over 500 cycles.

1. Introduction

Lithium-ion technology currently dominates electrochemical energy storage applications. Because of the scarcity of lithium and the impractical energy density of standard Li-ion batteries (LIB), researchers started to look beyond Li-ion technology. Moreover, high costs and limited lifetime so far impede their use in large-scale energy storage. On the other hand, high-temperature sodium-sulfur (HT Na-S) batteries with solid β-alumina electrolytes (760 Wh/kg) have been widely used for grid applications for almost two decades. However, working at high temperatures entails serious safety issues and operating costs [1–3]. Thus, research on room-temperature (RT) Na-S batteries with a theoretical gravimetric energy density of 1274 Wh/kg is gaining increasing attention.

The electrolytes used in such Na-S batteries strongly affect the reaction kinetics at the electrodes. Specifically, the salt used in the electrolyte governs both ion mobility and anode stability. So far, the choice of electrolyte salts for sodium-ion batteries (NIBs) is limited to $NaClO_4$, $NaPF_6$, $NaCF_3SO_3$, NaTFSI, NaFSI, $NaBF_4$, and $NaAsF_6$, which are analogous to the salts used in LIBs [4]. These salts suffer from disadvantages such as sensitivity towards moisture, limited electrochemical window, explosiveness ($NaClO_4$), corrosive behavior towards aluminum-based current collectors (NaTFSI, $NaCF_3SO_3$, NaFSI), or toxicity ($NaAsF_6$). Currently, RT Na-S batteries use similar electrolytes to NIBs [5–7], though with the limited overall performance of the final batteries. It is therefore essential to develop novel, stable, highly conductive, and non-corrosive electrolytes for RT Na-S batteries [8].

So far, the use of sulfur-based cathodes employing simple sulfur-carbon composites results in the formation of long-chain polysulfides upon reaction with sodium ions during discharge in ether-based electrolytes. These long-chain polysulfides are retained by carbon-based materials only through weak physical adsorption and can therefore easily dissolve in the electrolyte, which results in a severe polysulfide shuttle effect and self-discharge of the battery [9]. On the other hand, long-chain polysulfides react with carbonate-based electrolytes reducing the overall performance of the cell [10]. Several alternatives were considered to mitigate this phenomenon such as the formation of stable solid electrolyte interphases (SEIs), modifications of the cathode architecture or the separator, the use of tailored polymer electrolytes, or hosts to retain polysulfides [11–13]. In sulfurized poly(acrylonitrile) (SPAN) the sulfur is covalently bound to the composite backbone, which eliminates the above-mentioned issues [14] The use of SPAN in a RT Na-S

* Corresponding author.
E-mail address: michael.buchmeiser@ipoc.uni-stuttgart.de (M.R. Buchmeiser).

https://doi.org/10.1016/j.elecom.2021.107137
Received 18 August 2021; Received in revised form 22 September 2021; Accepted 30 September 2021
Available online 7 October 2021

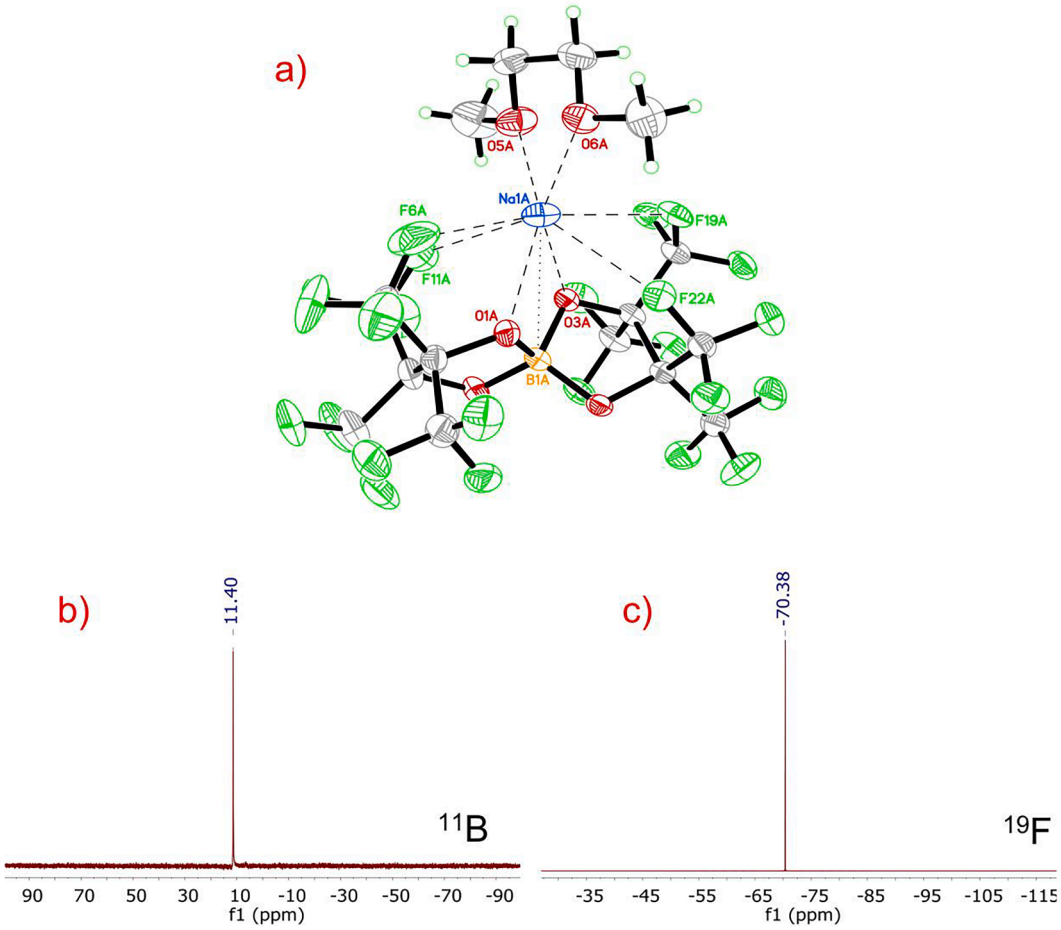

Fig. 1. a) Structure of Na-PPB as determined by single-crystal X-ray analysis; b) ^{11}B- and c) ^{19}F NMR spectra of Na-PPB in CD_3CN.

battery was first reported by Wang *et al.*, where the high compatibility of SPAN with the sodium anode and a high initial discharge capacity of 655 mAh/$g_{cathode}$ were demonstrated [15]. Since then, SPAN-based composite cathodes, together with different electrolytes, have been used for RT Na-S batteries [16–20].

Here, we outline the use of the sodium salt of a fluorinated, weakly coordinating anion (WCA), 'bis(perfluoropinacol) borate' (Na-PPB) as an electrolyte salt for SPAN-based RT Na-S batteries. It possesses a wide electrochemical window, a high oxidation potential, high solubility, and its chemical and electrochemical stability allows for realizing RT Na-S batteries with high discharge capacity and high coulombic efficiency.

2. Experimental

2.1. Synthesis of $Na[B(O_2C_2(CF_3)_4)_2]$ (Na-PPB)

A modified synthetic route under inert conditions was developed [21]. $NaBH_4$ (1 g, 26.43 mmol) was pulverized inside a glovebox and then transferred to a Schlenk flask filled with 50 mL of 1,2-dimethoxyethane (DME). The solution was cooled to 0 °C under constant stirring. Then, hexafluoro-2,3-bis(trifluoromethyl)-2,3-butanediol (18 g, 55.5 mmol) was added dropwise over a period of 1 h. After complete addition, the solution was slowly heated at 20 °C/h to reflux and then refluxed for 24 h. Then, DME was removed under vacuum followed by three-fold co-evaporation with pentane. The residuals were suspended in pentane and filtered. The final product was dried at RT under vacuum (10^{-3} mbar) for 24 h and 12 h under ultra-high vacuum (10^{-9} mbar) at 30 °C. A pure white salt was obtained in 90% yield. NMR (CD_3CN) and elemental analysis confirmed sufficient purity (Table S1, S.I.).

2.2. Cathode fabrication and electrochemical characterization

SPAN was synthesized according to the literature [21–22]. The cathode slurry was prepared by mixing 70 wt% SPAN, 20 wt% carbon black, and 10 wt% Na-CMC binder in water using a planetary mixer (Thinky, Japan) and coating on a carbon-coated aluminum foil with a wet thickness of 300 μm. The final sulfur content in SPAN was 40.12 wt % (Table S2, S.I.). The average sulfur loading per cathode was 0.73 mg. Cell fabrication was carried out inside an Ar-filled glove box with Swagelok-T-type cells. 1 M Na-PPB in propylene carbonate with 10 wt% fluoroethylene carbonate (FEC) was used as an electrolyte. For linear-sweep voltammetry (LSV) (using Biologic VMP3) carried out at 1 mV s^{-1}, sodium metal was used both as a reference and counter electrode employing different metal sheets as working electrodes (Pt, Cu, Al, SS, and Al/C). The sodium metal was cut from the block, rolled to the desired thickness and then punched into 12 mm discs. Full Na-SPAN cells were fabricated by placing the following in order: sodium anode, two glass fiber separators, and SPAN cathode. The potential window for cyclic voltammetry (CV) was set between 0.5 and 3 V using a scan rate of 0.1 mV s^{-1}. Galvanostatic cycling and rate capability testing (one pre-formation cycle at 0.3 C) were carried out on a BasyTec XCTS-LAB systems, Germany, at 2C and 1–4C, respectively, using a voltage window between 0.5 and 3 V vs. Na/Na^+.

2.3. Density functional calculations

Binding energies of the Na-PPB and the Na-hfip salt were calculated with the Gaussian 09 software [23] package using density functional theory. The initial geometries were optimized at the B3LYP/6-31 + G

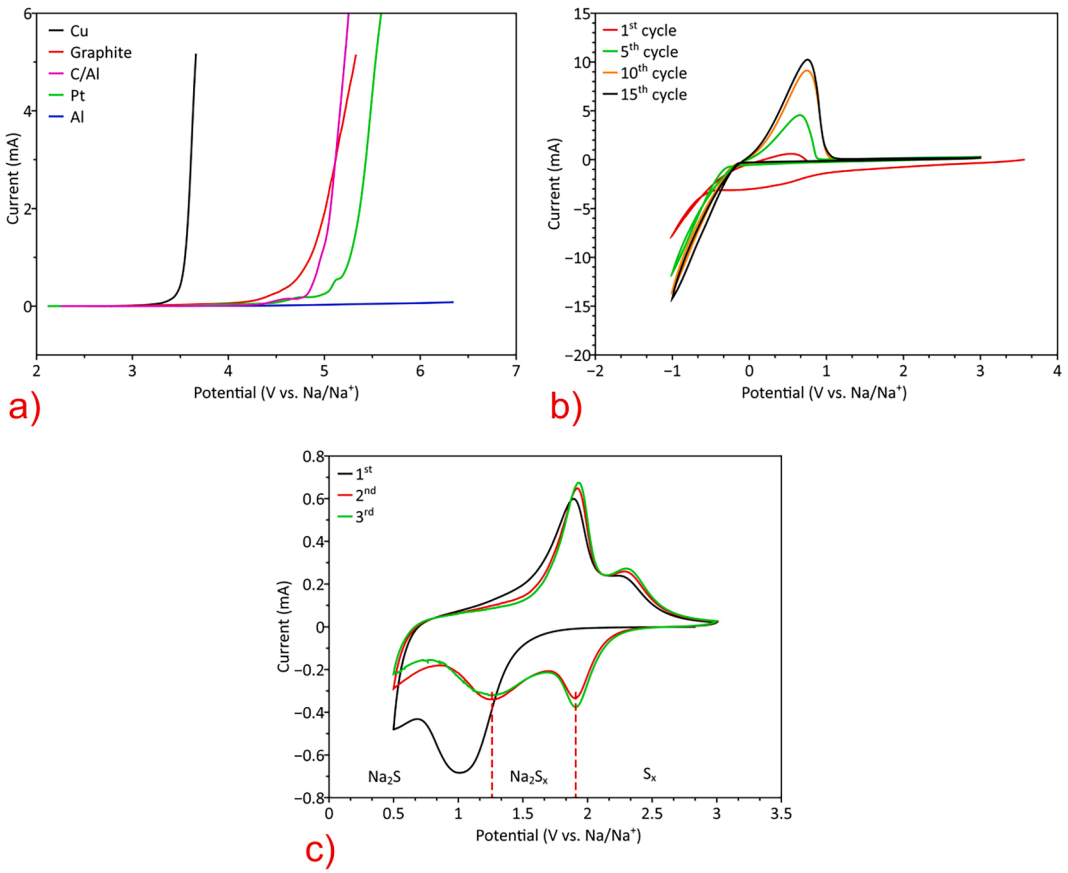

Fig. 2. Electrochemical performance of a Na-PPB-based electrolyte measured with Na as counter and reference electrode, a) LSV of different working electrodes scanned at 1 mV s^{-1} with Cu (black), graphite (red), carbon-coated aluminum (pink), Pt (green), and Al (blue); b) plating and stripping test with graphite as working electrode scanned at 1 mV s^{-1} showing the 1st (red), 5th (green), 10th (orange), and 15th (black) cycle; and c) CV of a Na-SPAN full cell recorded at 0.1 mV s^{-1} at the 1st (black), 2nd (red), and 3rd (green) cycle. (For interpretation of the references to colour in this figure legend, the reader is referred to the web version of this article.)

(2d,p) level. On these optimized geometries, single-point energies were calculated at the B3LYP/6-311 + G(2df,2p) level. Binding energies include zero-point vibrational energies (ZPE). Reaction paths were obtained by performing nudged elastic band (NEB) calculations at the B3LYP-D3(BJ)/def2-SVP level in Turbomole V.7.4 [24] performed in ChemShell [25–26] via DL-FIND [27].

3. Results and discussion

3.1. Synthesis and characterization of Na-PPB

The pK_a value of perfluoropinacol (5.95 vs. 18 for pinacol) facilitates the deprotonation by $NaBH_4$ [28]. The reaction between $NaBH_4$ and perfluoropinacol resulted in Na-PPB in 90% isolated yield. Na-PPB was analyzed by single-crystal X-ray analysis, NMR, and elemental analysis to ensure purity. Single crystals formed by slowly diffusing pentane into a chloroform solution of Na-PPB at −30 °C. Single-crystal X-ray analysis showed that the unit cell contains one DME-solvated Na^+ ion weakly coordinated to four fluorine and two oxygen atoms of the counter anion (Fig. 1a). The boron atom is coordinated by two bidentate perfluoropinacolate groups. The ^{11}B and ^{19}F NMR spectra show signals at δ = 11.40 and δ = 70.38 ppm, respectively, in line with the results of single-crystal X-ray analysis (Fig. 1b and 1c).

3.2. Electrochemical characterization

The oxidative stability of the electrolyte was determined by linear sweep voltammetry (LSV) applying a potential sweep at the rate of 1 mV s^{-1}. As shown in Fig. 2a, the Na-PPB-based electrolyte exhibited remarkable oxidative stability on Al (>5.5 V) compared to Cu (3.25 V). Carbon-coated aluminum foil, Pt, and graphite showed oxidation stabilities of 4.58 V, 4.5 V, and 4.25 V, respectively. The high oxidation potential of Na-PPB by far surpasses other commercially available sodium salts used in the literature (Table S3) [11,29]. The resistance of Na-PPB towards oxidation is attributed to the presence of the electron-withdrawing CF_3 groups, which reduce the electron density at both, carbon and boron, and lower the HOMO level, corroborating the results from Fig. S1 (S.I.) [30]. The plating and stripping behavior of the Na–PPB-based electrolyte on a graphite electrode strongly improved during the first 10 cycles (Fig. 2b). The overpotentials during plating and stripping at the 5th cycle were −0.26 V and −0.13 V, respectively. Further cycling resulted in a decreased plating overpotential (-0.17 V for the 10th cycle and −0.14 V for the 15th cycle) and increased current density. This enhancement in plating is attributed to the deposition of Na onto Na nucleated during the first cycle. Finally, a full cell using Na-SPAN as cathode was assembled for CV measurements. During the first cycle (Fig. 2c), only one reduction peak was observed at 1 V, which was shifted to a higher potential (1.92 V) during the 2nd cycle with the appearance of a new peak at 1.25 V. The first reduction peak indicates the reduction of sulfur in the SPAN backbone to form short-chain polysulfide intermediates at 1.92 V, followed by sodiation at 1.25 V to give the final discharge product Na_2S [31]. Similarly, during charging, the formed sulfides are reoxidized to short-chain sulfides at 1.92 V, which then reattach to the SPAN backbone at 2.3 V.

To show the electrochemical performance of the Na-PPB-based electrolyte in a Na-SPAN full cell, both stress tests and long-term

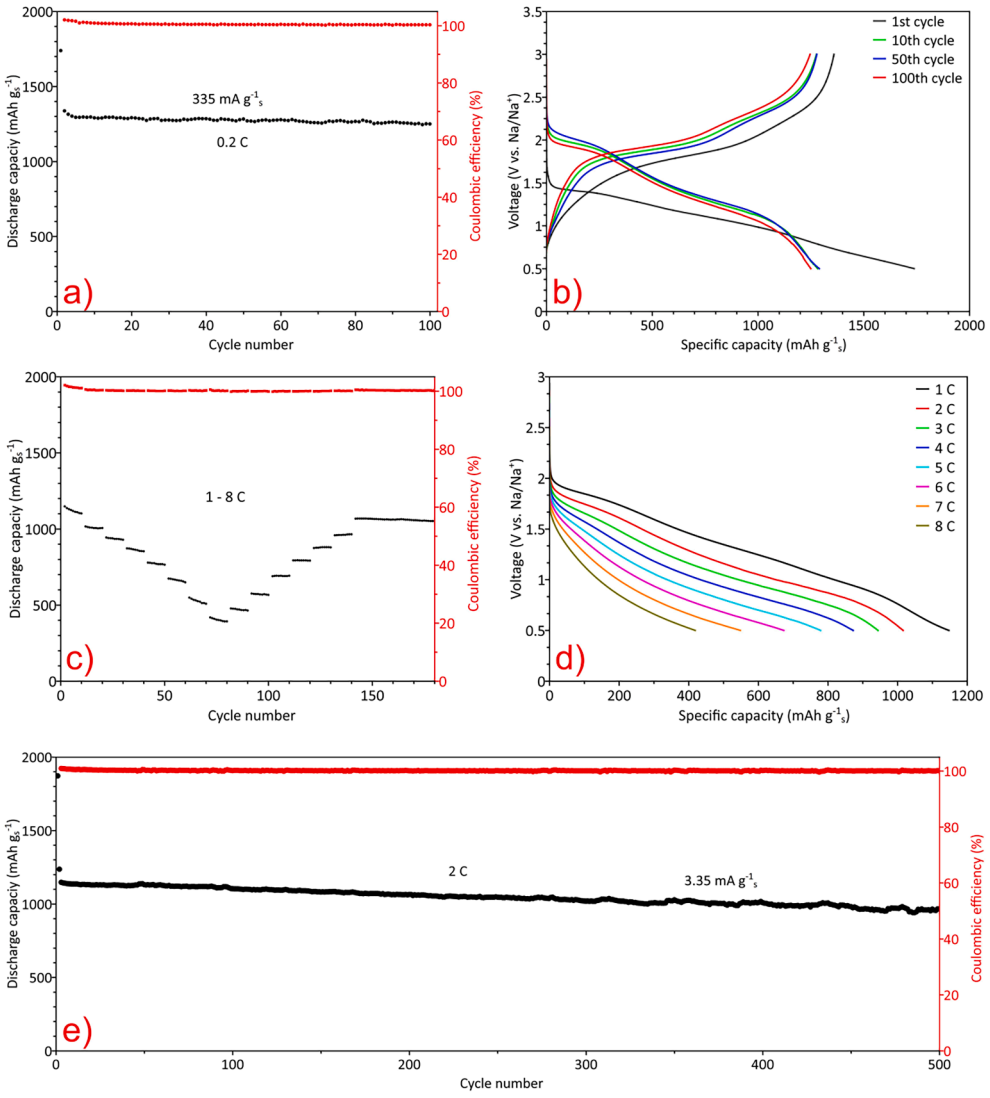

Fig. 3. Galvanostatic cycling measurements of a Na-SPAN full cell with a Na-PPB-based electrolyte, a) cycling at low C-rate (0.2C) for 100 cycles; b) voltage profiles at 0.2C during the 1st (black), 10th (green), 50th (blue), and 100th (red) cycle; c) stress test performed between 1 and 8C and the corresponding voltage profiles of the first cycle at each C-rate (d); e) long term cycling at 2C, discharge capacity (black) and coulombic efficiency (red) for the first 500 cycles. (For interpretation of the references to colour in this figure legend, the reader is referred to the web version of this article.)

cycling were carried out under defined conditions. Cells were cycled against Na metal between 0.5 and 3 V at a low C-rate (0.2C). The discharge capacity curve (Fig. 3a) showed high capacity (>1250 mAh/g_{sulfur}), indicating full conversion of SPAN-bound sulfur to Na_2S/Na_2S_2. During the first cycle (Fig. 3b) irreversible Na^+ insertion, SEI layer formation, and irreversible reduction of short conjugated carbon bonds in SPAN fragments lead to high initial discharge capacity (1738 mAh/g_{sulfur}) [32–34]. The voltage vs. specific capacity curve revealed two distinct discharge plateaus at 1.9 V and 1.1 V, implying multi-step conversion reactions. The overpotential decreased upon cycling until the 50th cycle, then insignificantly increased at the 100th cycle, demonstrating high compatibility of the Na-PPB electrolyte with both Na and SPAN cathode. Upon cycling at high C-rates of 1C up to 8 C the full Na-SPAN cell demonstrated 1147, 1016, 943, 872, 778, 673, 548, and 418 mAh/g_{sulfur}, respectively (Fig. 3c and d). During reversal to the initial C-rate (1C), the capacity almost fully restored to the initial value (1067 mAh/g_{sulfur}, suggesting high-stress endurance of the cathode and the electrolyte. Fig. 3e shows the long-term galvanostatic cycling at 2C. The Na-PPB-based electrolyte showed a stable and high initial discharge capacity of 1146 mAh/g_{sulfur} and maintained > 950 mAh/g_{sulfur} for 500 cycles with an average capacity decay of 0.016 % per cycle. The cell maintained an average coulombic efficiency of 99.8%. This high performance of the Na-SPAN cell shows that Na-PPB salt is electrochemically stable.

Unlike a monodentate ligand-containing salt such as sodium tetrakis (hexafluoroisopropyloxy) borate $NaB[OH(CF_3)_2]_4$ (Na-hfip), Na-PPB is chemically stable due to its unique structure based on a bidentate ligand. We conducted a symmetrical Na || Na test to compare the overpotential of both salts. No significant differences in overpotential were observed except for a high plating overpotential of the Na-hfip salt (Fig. S2a and S2b, S.I.). The coulombic efficiency during stripping and plating of Na was calculated by chronopotentiometry analysis. A constant high cathodic current density of 1 mA cm^{-2} was applied until the capacity reached 0.5 mAh cm^{-2} and an anodic current of 1 mA cm^{-2} was applied until the potential reached 1 V. Fig. S3a (S.I.) shows a coulombic efficiency during the first cycle of ~ 50%, which increased up to 89.5% after the 50th cycle. Fig. S3b (S.I.) shows an insignificant increase in overpotential during cycling, indicating that the Na-PPB electrolyte had stable Na plating/striping potentials. Na-PPB exhibited exceptionally high stability under atmospheric conditions. To analyze the hydrolysis resistance of salts, we kept both salts in the air for 20 days. Upon addition of CD_3CN, Na-PPB formed a clear solution whereas, Na-hfip was partially insoluble resulting in a milky white solution. Partially insoluble particles suggest a decomposition reaction that occurred between the salt and atmospheric moisture. Fig. S4a and b (S.I.) show the ^{19}F NMR spectra of both salts exposed to air for 20 days. Na-PPB still showed a single peak whereas Na-hfip showed a new fluorine peak at δ = -75.9 ppm, indicating the formation of decomposition products. We

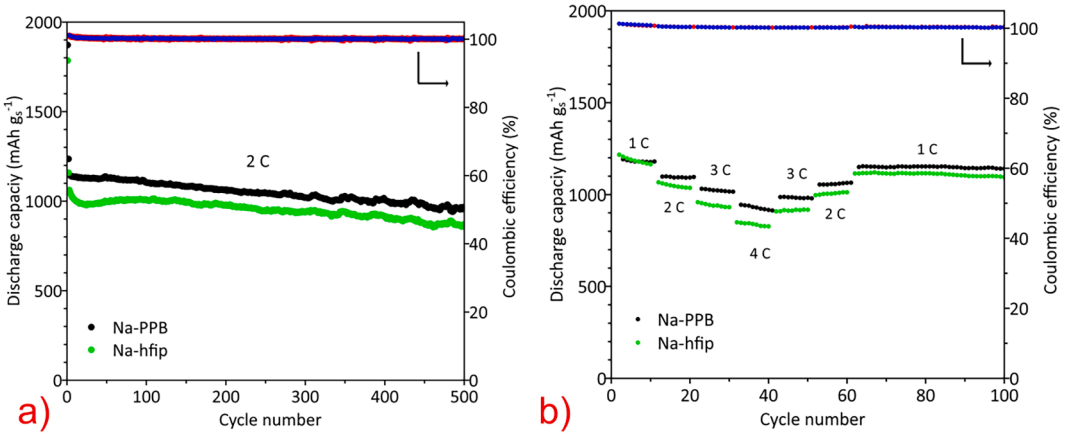

Fig. 4. Galvanostatic test comparison between a Na-PPB and a Na-hfip based electrolyte, a) long term cycling at 2C; b) rate capability assessment performed between 1 and 4C.

Table 1
Binding energies E_{bind} of the WCA with the Na^+ cation in Na-PPB and Na-hfip.

Compound	E_{bind} in kJ•mol^{-1}
Na-PPB	−369.4
Na-hfip	−374.6

attribute this high stability of the Na-PPB salt to the thermodynamic stability of bidentate over monodentate ligands [35]. Salt decomposition and morphological changes were analyzed in detail by comparing both salts before and after exposure to air for 20 days (Tables S4 and S5, S.I.).

3.3. Theoretical analysis

A comparison of the galvanostatic electrochemical tests for the Na-PPB and Na-hfip electrolyte, respectively, revealed a lower capacity and lower stress endurance of the Na-hfip salt-based electrolyte (Fig. 4a and b). Generally, the Na^+ ion mobility in an electrolyte, which is fostered by the use of WCAs, plays an important role in the conversion reaction that occurs on the cathode. To elucidate the better performance of the Na-PPB salt-based electrolyte, density functional (DFT) calculations were carried out to investigate the energy needed for Na^+ ion movement. The binding energies of Na^+ solvated by DME to the PPB and hfip anion, respectively, were calculated (Table 1). The small difference in the binding energy of 5.2 kJ mol^{-1} between the Na-PPB and the Na-hfip salt, however, does not explain the better performance of the Na-PPB salt-based electrolyte.

Hence, we compared the barriers responsible for Na^+ mobility in the electrolyte. The relevant re-orientation is the movement of Na^+ around the anion. To receive a minimum energy path (MEP) on the potential energy surface (PES) between two local minima of the coordination to the anions, NEB calculations of both the Na-PPB and the Na-hfip based electrolyte were performed (Fig. S5, S.I.). Interestingly, the barrier for Na^+ ion movement within the Na-hfip electrolyte is rather high (136.9 kJ mol^{-1}), which leads to a decreased Na^+ mobility. In contrast, for the Na-PPB electrolyte, the barrier is significantly lower (74.3 kJ mol^{-1}) and can easily be overcome at room temperature, which results in higher Na^+ ion mobility and, consequently, in a better electrochemical performance.

To analyze the effect of salt hydrolysis on electrochemical performance, both Na-PPB and Na-hfip were left under ambient atmospheric conditions for two days in a petri dish. The electrolytes were prepared by adding propylene carbonate and 10 wt% FEC to the corresponding salt under constant stirring. Insoluble particles of the Na-hfip salt were filtered off before injecting the solution into the cell. Rapid degradation of the Na-hfip cell was observed in the discharge curve (Fig. 5a), indicating decomposed Na-hfip adversely affects the cell performance. By contrast, the Na-PPB-based cell showed high rate capability and stable cycling. The voltage profile (Fig. 5b) confirmed the reduced overpotential of the Na-PPB electrolyte, illustrating good electrochemical

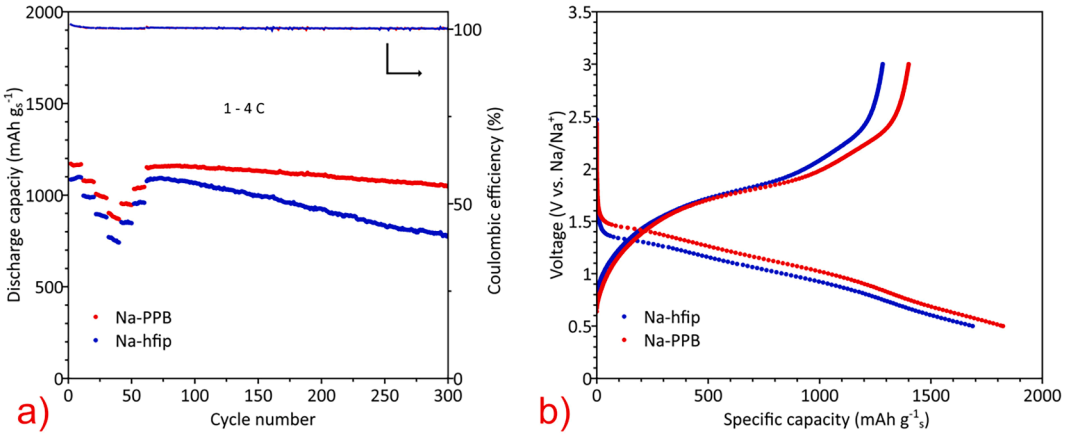

Fig. 5. Electrochemical analysis of Na-PPB and Na-hfip after exposure to air for 2 days, a) rate performance of Na-PPB (red) and Na-hfip (blue) between 1 and 4C; b) voltage profile of both salts during the first discharge and charge cycle. (For interpretation of the references to colour in this figure legend, the reader is referred to the web version of this article.)

reaction kinetics compared to Na-hfip.

4. Conclusions

In summary, a new type of electrolyte salt based on a weakly coordinating anion (Na-PPB) for RT Na-SPAN batteries has been developed. Na-PPB was synthesized in bulk via a one-pot reaction. NMR spectroscopy reveals high purity of the salt and stability even under ambient atmospheric conditions. Single-crystal X-ray analysis confirmed the molecular structure of Na-PPB with Na^+ coordinated by one DME molecule. The electrolyte containing Na-PPB with PC + 10 wt% FEC showed high oxidative stability on Al current collector exceeding 5.5 V. In a Na-SPAN cell, the Na-PPB electrolyte allows for an initial and final discharge capacity (500 cycles) of 1140 mAh/g_{sulfur} and 965 mAh/g_{sulfur} respectively, obtained at 2C (3.35 A/g_{sulfur}). The excellent electrochemical performance and good chemical stability of Na-PPB offers access to the design of novel electrolyte salts for RT Na-SPAN batteries.

CRediT authorship contribution statement

Saravanakumar Murugan: Conceptualization, Data curation, Formal analysis, Investigation, Methodology, Validation, Visualization, Writing – original draft, Writing – review & editing. **Sina V. Klostermann:** Data curation, Formal analysis, Validation, Visualization, Writing – review & editing. **Wolfgang Frey:** Data curation, Formal analysis. **Johannes Kästner:** Funding acquisition, Resources, Supervision. **Michael R. Buchmeiser:** Funding acquisition, Methodology, Project administration, Resources, Supervision, Validation, Writing – original draft, Writing – review & editing.

Declaration of Competing Interest

The authors declare that they have no known competing financial interests or personal relationships that could have appeared to influence the work reported in this paper.

Acknowledgments

We gratefully acknowledge funding and support from the German Federal Ministry for Economic Affairs and Energy [BMWi, project no. S50400, *FiMaLiS*]. We thank the Deutsche Forschungsgemeinschaft [DFG, German Research Foundation] for supporting this work by funding – [EXC2075 – 390740016] under Germany's Excellence Strategy. We acknowledge the support of the Stuttgart Center for Simulation Science (SimTech). The authors also acknowledge support by the State of Baden-Württemberg through bwHPC and the German Research Foundation (DFG) through grant no [INST 40/575-1 FUGG (JUSTUS 2 cluster)].

Appendix A. Supplementary data

Supplementary data to this article can be found online at https://doi.org/10.1016/j.elecom.2021.107137.

References

[1] S.S. Berbano, I. Seo, C.M. Bischoff, K.E. Schuller, S.W. Martin, J. Non-Cryst, Solids 358 (2012) 93–98.
[2] K. Hueso, M. Armand, T. Rojo, Energy Environ. Sci. 6 (2013) 734–749.
[3] R. Okuyama, H. Nakashima, T. Sano, E. Nomura, J. Power Sources 93 (2001) 50–54.
[4] V. Aravindan, J. Gnanaraj, S. Madhavi, H.-K. Liu, Chem. Eur. J. 17 (2011) 14326–14346.
[5] S. Zhang, Y. Yao, Y. Yu, ACS Energy Lett. 6 (2021) 529–536.
[6] Y.-X. Wang, B. Zhang, W. Lai, Y. Xu, S.-L. Chou, H.-K. Liu, S.-X. Dou, Adv. Energy Mater. 7 (2017) 1602829.
[7] Y. Wang, Y. Zhang, H. Cheng, Z. Ni, Y. Wang, G. Xia, X. Li, X. Zeng, Molecules 26 (2021) 1535.
[8] S. Murugan, S. Niesen, J. Kappler, K. Küster, U. Starke, M.R. Buchmeiser, Batter. Supercaps, https://doi.org/10.1002/batt.202100125.
[9] B. Zhang, J. Wu, J. Gu, S. Li, T. Yan, X.-P. Gao, ACS Energy Lett. 6 (2021) 537–546.
[10] T. Yim, M.-S. Park, J.-S. Yu, K.J. Kim, K.Y. Im, J.-H. Kim, G. Jeong, Y.N. Jo, S.-G. Woo, K.S. Kang, I. Lee, Y.-J. Kim, Electrochim. Acta 107 (2013) 454–460.
[11] X. Xu, D. Zhou, X. Qin, K. Lin, F. Kang, B. Li, D. Shanmukaraj, T. Rojo, M. Armand, G. Wang, Nat. Commun. 9 (2018) 3870.
[12] N. Wang, Y. Wang, Z. Bai, Z. Fang, X. Zhang, Z. Xu, Y. Ding, X. Xu, Y. Du, S. Dou, G. Yu, Energy Environ. Sci. 13 (2020) 562–570.
[13] S. Wei, S. Xu, A. Agrawral, S. Choudhury, Y. Lu, Z. Tu, L. Ma, L.A. Archer, Nat. Commun. 7 (2016) 11722.
[14] T. Lebherz, M. Frey, A. Hintennach, M.R. Buchmeiser, RSC Adv. 9 (2019) 7181–7188.
[15] J. Wang, J. Yang, Y. Nuli, R. Holze, Electrochem. Commun. 9 (2007) 31–34.
[16] Z. Li, J. Zhang, Y. Lu, X. Lou, Sci. Adv. 4 (2018) 1687.
[17] L. Wang, X. Chen, S. Li, J. Yang, Y. Sun, L. Peng, B. Shan, J. Xie, J. Mater. Chem. A (2019) 7.
[18] X. Chen, L. Peng, L. Wang, J. Yang, Z. Hao, J. Xiang, K. Yuan, Y. Huang, B. Shan, L. Yuan, J. Xie, Nat. Commun. 10 (2019) 1021.
[19] S. Ma, P. Zuo, H. Zhang, Z. Yu, C. Cui, M. He, G. Yin, Chem. Commun. 55 (2019) 5267–5270.
[20] Y. Hu, B. Li, X. Jiao, C. Zhang, X. Dai, J. Song, Adv. Funct. Mater. 28 (2018) 1801010.
[21] S. Bulut, P. Klose, I. Krossing, Dalton Trans. 40 (2011) 8114–8124.
[22] M. Frey, R. Zenn, S. Warneke, K. Küster, A. Hintennach, R. Dinnebier, M. Buchmeiser, ACS Energy Lett. (2017) 2.
[23] M. J. Frisch, G. W. Trucks, H. B. Schlegel, G. E. Scuseria, M. A. Robb, J. R. Cheeseman, G. Scalmani, V. Barone, G. A. Petersson, H. Nakatsuji, X. Li, M. Caricato, A. V. Marenich, J. Bloino, B. G. Janesko, R. Gomperts, B. Mennucci, H. P. Hratchian, J. V. Ortiz, A. F. Izmaylov, J. L. Sonnenberg, Williams, F. Ding, F. Lipparini, F. Egidi, J. Goings, B. Peng, A. Petrone, T. Henderson, D. Ranasinghe, V. G. Zakrzewski, J. Gao, N. Rega, G. Zheng, W. Liang, M. Hada, M. Ehara, K. Toyota, R. Fukuda, J. Hasegawa, M. Ishida, T. Nakajima, Y. Honda, O. Kitao, H. Nakai, T. Vreven, K. Throssell, J. A. Montgomery Jr., J. E. Peralta, F. Ogliaro, M. J. Bearpark, J. J. Heyd, E. N. Brothers, K. N. Kudin, V. N. Staroverov, T. A. Keith, R. Kobayashi, J. Normand, K. Raghavachari, A. P. Rendell, J. C. Burant, S. S. Iyengar, J. Tomasi, M. Cossi, J. M. Millam, M. Klene, C. Adamo, R. Cammi, J. W. Ochterski, R. L. Martin, K. Morokuma, O. Farkas, J. B. Foresman, D. J. Fox, Wallingford, CT, 2016.
[24] S.G. Balasubramani, G.P. Chen, S. Coriani, M. Diedenhofen, M.S. Frank, Y. J. Franzke, F. Furche, R. Grotjahn, M.E. Harding, C. Hättig, A. Hellweg, B. Helmich-Paris, C. Holzer, U. Huniar, M. Kaupp, A.M. Khah, S.K. Khani, T. Müller, F. Mack, B. D. Nguyen, S.M. Parker, E. Perlt, D. Rappoport, K. Reiter, S. Roy, M. Rückert, G. Schmitz, M. Sierka, E. Tapavicza, D.P. Tew, C.V. Wüllen, V.K. Voora, F. Weigend, A. Wodyński, J.M. Yu, J. Chem. Phys. 152 (2020), 184107.
[25] P. Sherwood, A.H. de Vries, M.F. Guest, G. Schreckenbach, C.R.A. Catlow, S. A. French, A.A. Sokol, S.T. Bromley, W. Thiel, A.J. Turner, S. Billeter, F. Terstegen, S. Thiel, J. Kendrick, S.C. Rogers, J. Casci, M. Watson, F. King, E. Karlsen, M. Sjøvoll, A. Fahmi, A. Schäfer, C. Lennartz, J. Mol. Struct. 632 (2003) 1–28.
[26] S. Metz, J. Kästner, A.A. Sokol, T.W. Keal, P. Sherwood, Wiley Interdiscip. Rev. Comput. Mol. Sci. 4 (2014) 101–110.
[27] J. Kästner, J.M. Carr, T.W. Keal, W. Thiel, A. Wander, P. Sherwood, J. Phys. Chem. A 113 (2009) 11856–11865.
[28] J. Luo, Y. Bi, L. Zhang, X. Zhang, T.L. Liu, Angew. Chem. 58 (2019) 6967–6971.
[29] J. Wu, J. Liu, Z. Lu, K. Lin, Y.-Q. Lyu, B. Li, F. Ciucci, J.-K. Kim, Energy Storage Mater. 23 (2019) 8–16.
[30] K.-C. Lau, T. Seguin, E. Carino, N. Hahn, J. Connell, B. Ingram, K. Persson, K. Zavadil, C. Liao, J. Electrochem. Soc. 166 (2019) A1510–A1519.
[31] A.Y.S. Eng, D.-T. Nguyen, V. Kumar, G.S. Subramanian, M.-F. Ng, Z.W. Seh, J. Mater. Chem. A 8 (2020) 22983–22997.
[32] Z.-Q. Jin, Y.-G. Liu, W.-K. Wang, A.-B. Wang, B. Hu, M. Shen, T. Gao, P.-C. Zhao, Y.-S. Yang, Energy Storage Mater. (2018) 14.
[33] W. Wang, Z. Cao, G. Elia, W. Wahyudi, E. Abou-hamad, A.-H. Emwas, L. Cavallo, L. Li, ACS Energy Lett. 3 (2018).
[34] S. Zhang, Energies 7 (2014) 4588–4600.
[35] A.N. Srivastva, Stability and Applications of Coordination Compounds, Intech, 2020.